Study on the Organic Nanoparticles for Sustainable Energy Using Computational Simulations

Abstract

In the contemporary fuel cell technology, carbon-based nano-scaled materials display great potential to improve fuel efficiency and reduce the cost. However, their relatively low activity limits the development and application of photovoltaic cells. In this study, capacitors and computationally constructed CNT(carbon nanotube) with MOFs(metal–organic frameworks) composites were studied to evaluate their thermodynamic and electrical efficiencies. To examine the efficiencies of the components used in current photovoltaic cells, possible nano-composites using computational analysis were constructed and tested for their efficacies. Both theoretical calculations for different geometries and the computer simulations were performed to find the electrochemical properties in the nano-scaled materials. The stereo-chemical and thermo-dynamical properties were also found and analyzed.

1. Introduction

An alternative energy source for future generation, fuel cell technology, is perceived as a means of new energy production. However, fuel cell technology has problems that prohibit the growth and advancement in fuel cell commercialization. Therefore, in recent years, potential solutions in applications-related fuel cell technology use hydride complexes, as they are believed to be able to safely store large quantity of H_2. [1]

In particular, researchers have discovered several types of B_xH_y and Al_xH_y systems. This new discovery has sparked experimental and computational studies on $(BH_3)_n$ and $(AlH_3)_n$ clusters. The high volumetric hydrogen capacity allows borane and alane complexes to be an appropriate potential hydrogen storage material. At room temperature, BH_3 and AlH_3, a metastable solid, embody several polymorphs that share common structural features of six hydrogen atoms encircling a boron and an aluminum atom in an octahedral formation (AlH_6) respectively. However, the ways in which the borons bridge together to form a polymeric solid are unique in each polymorph.[2]

In the light of the promising use of borane and alane complexes, we wanted to study their thermodynamic stability. For this purpose, we used the program Avogadro to model, optimize, and compare the resulting molecular energy of the clusters. Additionally for $(AlH_3)_n$ clusters, we compare our results to Kiran's paper from which we first learned about the cluster structures and their energy comparisons. [3]

2. Materials and Methods

This project aims to determine the optimized energy of the hydride compounds using a computational chemistry method, specifically with the chemical program Avogadro. [4] Avogadro is an open-source molecular editing program with an auto-optimization feature that determines the theoretical values of the structure's atomic properties. It allows users to

build virtually any molecule with the optimized geometry according to various force field options. While UFF (Universal Force Field) is suitable for optimizing most molecules, we first optimized our molecules with GAFF (General Amber Force Field) and then with UFF. This approach often produced lower molecular energy and more regular geometry than optimization with UFF alone. In addition, we modeled each 3-center-2-electron bond (M-H-M, where M=metal) as two single bonds in Avogadro, since we are not aware of any feature in Avogadro that supports creation of 3-center-2-electron bonds. [5]

To define the efficiencies of the nanoparticles, three factors must be considered. The first factor is thermodynamic stability. This factor can be measured by the optimized energy of the molecule. The smaller the optimized energy, the better its thermodynamic stability.

The second factor is reactivity, activity, or conductivity. This factor can be measured by the dipole moment. The higher the dipole moment is, the better reactivity the molecule has. The third factor is the electrostatic potential map. A colorful electrostatic potential map means that the molecule has a higher electrostatic potential, which leads to the conclusion of high reactivity. [6]

3. Data and Results

3.1 A Plate Capacitor Filled with a Dielectric

A slab of width d and dielectric constant K is inserted at a distance x between the square parallel plates (of side l) of a capacitor as shown in [Fig. 1].

A simulation using MATLAB computer programming to calculate the capacitances and electric fields of capacitors were performed. To find the relationship between change in the capacitances and electric fields of capacitors (dC and dE) of the capacitor, and x (the distance inserted in the system), the following distributions were obtained.

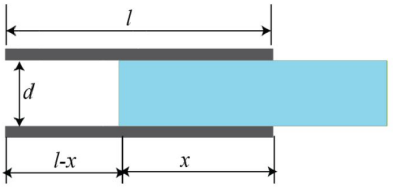

(a)

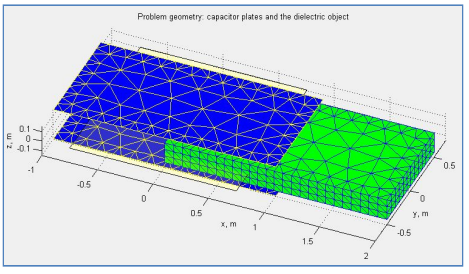

(b)

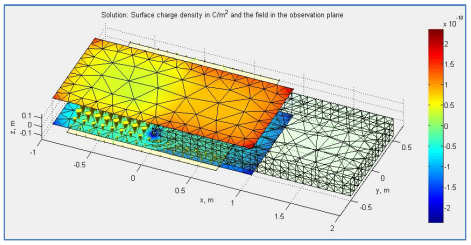

(c)

[Fig. 1] A capacitor inserted with a dielectric - Calculation of dC and dE of the capacitors as the distance inserted in the system changes, (a) Slab with plates (b) Mesh generation (c) Electric field distribution

First, let's determine the capacitance and then the energy stored as a function of x.

$$C = C_{air} + C_{dielectric} \qquad \text{(Eq. 1)}$$

$$= \frac{\epsilon_0 l(l-x)}{d} + \frac{K\epsilon_0 lx}{d} \qquad \text{(Eq. 2)}$$

The internal energy of the system can be easily found as follows:

$$U = \frac{1}{2}CV_0^2 = (\frac{\epsilon_0 l^2 V_0^2}{2d})(1 + (K-1)(\frac{x}{l})) \qquad \text{(Eq. 3)}$$

The potential, charges, electric fields along x, y and z axis were found as they are shown in the [Table 1]:

[Table 1] Potential, charges and electric fields in the capacitor

Name	Value
Numerical capacitance,pF	169.9453
Total charge of the first conductor, C	-1.6995e-10
Total charge of the second conductor, C	1.6995e-10
Total charge of the dielectric object, C	1.1246e-25
Sum of charges for the entire structur...	-1.6792e-26
E field x component at obs. point, V/m	2.8012e-05
E field y component at obs. point, V/m	-0.0012
E field z component at obs. point, V/m	-0.5521
Electric potential at obs. point, V	-5.7261e-06
Number of triangular patches in the me...	368
Number of triangular patches in the diel...	824
Minimum triangle quality in the mesh	0.6082
CPU time in sec for filling the MoM matrix	14.0156
CPU time in sec for solving the system ...	0.2813

3.2 Cylindrical Shell Capacitor

A thin-walled hollow cylinder capacitor filled with 2 dielectrics with concentric shells of radii r1, r2 and r3 respectively.

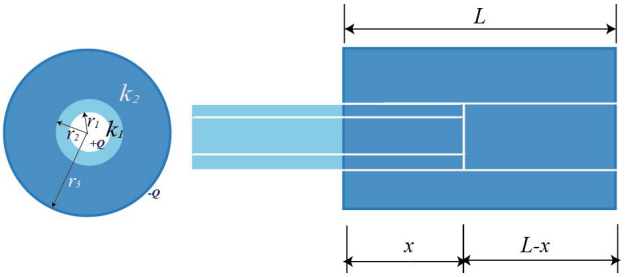

[Fig. 2] A thin walled hollow cylinder

A thin-walled hollow cylinder(k1) is concentric with a solid cylinder(k2) with radius $r_a < r_b$. Each has length L.

By changing the insertion distance x, the capacitance and the amount of charge stored in the system can be adjusted. Let's find the capacitance as a function of x. expressing the capacitance in terms of r_1, r_2, r_3 , k, L, x, epsilon and pi.

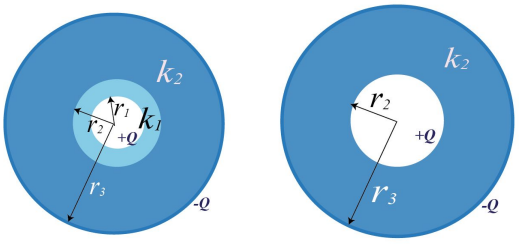

(a) Section *x* (b) Section *L-x*

[Fig. 3] Cross sections of the hollow cylinder

$$C = C_A + C_B$$

$$= \frac{k_2 ln\frac{r_2}{r_1} + k_1 ln\frac{r_3}{r_2}}{2\pi\epsilon_0 k_1 k_2 x} + (L-x)(\frac{2\pi\epsilon_0 k_2}{ln\frac{r_3}{r_2}})$$

Or the C can be expressed as a function of x

$$C = \frac{k_2 ln\frac{r_2}{r_1} + k_1 ln\frac{r_3}{r_2}}{2\pi\epsilon_0 k_1 k_2 x} + (L-x)(\frac{2\pi\epsilon_0 k_2}{ln\frac{r_3}{r_2}})$$

$$C = [\frac{k_2 ln\frac{r_2}{r_1} + k_1 ln\frac{r_3}{r_2}}{2\pi\epsilon_0 k_1 k_2}](\frac{1}{x}) + (L-x)(\frac{2\pi\epsilon_0 k_2}{ln\frac{r_3}{r_2}})$$

The energy stored is

$$U = \frac{1}{2}CV_0^2 = \frac{1}{2}[\frac{k_2 ln\frac{r_2}{r_1} + k_1 ln\frac{r_3}{r_2}}{2\pi\epsilon_0 k_1 k_2 x} + (L-x)(\frac{2\pi\epsilon_0 k_2}{ln\frac{r_3}{r_2}})]V_0^2$$

When the slab moves a small distance d*x*, the capacitance change is

$$dC = \frac{k_2 ln\frac{r_2}{r_1} + k_1 ln\frac{r_3}{r_2}}{2\pi\epsilon_0 k_1 k_2}(\frac{-1}{x^2}) + L(\frac{2\pi\epsilon_0 k_2}{ln\frac{r_3}{r_2}}) - (\frac{2\pi\epsilon_0 k_2}{ln\frac{r_3}{r_2}})$$

We see that there is an increase in the energy stored in the capacitor:

$$dU_{capacitor} = \frac{1}{2}[\frac{k_2 ln\frac{r_2}{r_1} + k_1 ln\frac{r_3}{r_2}}{2\pi\epsilon_0 k_1 k_2}(\frac{-1}{x^2}) + L(\frac{2\pi\epsilon_0 k_2}{ln\frac{r_3}{r_2}}) - (\frac{2\pi\epsilon_0 k_2}{ln\frac{r_3}{r_2}})]V_0^2$$

3.3 Photovoltaic Cell and Nanoparticles in the photoactive layer

In the photovoltaic cell, subsequent charge separation in the interface between an electron donor and acceptor blend within the device's active layer.

In the following sections, potential nanoparticles such as alane, borane, CNTs and MOFs that can be used as electron donors and acceptors in the active layer are analyzed.

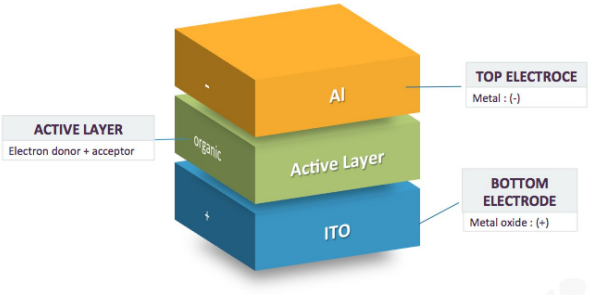

[Fig. 4] Organic polymer molecules in active layer are randomly dispersed before they are polarized to electron donors and acceptors in the cells

3.4 Optimized Energy of Alane Clusters$(AlH_3)_n$

Various clusters of AlH_3 were created in Avogadro. The resulting optimized energy is given in the [Table 2] and [Fig. 5] Their structures obtained from optimization in Avogadro are given in [Fig. 6] . The names of the isomers are as shown in Kiran's paper.[7]

As complexity increases, the optimized energy increases as well, albeit with increased variation within the cluster.

Unlike Kiran's study which found that isomers with hexa-coordinate Al atoms (4a, 5a, 6a, 7a, and especially 8a) are the most energetically preferred, the isomers with the lowest optimized energy (4b, 5d, 6b, 7d, and 8a) in our study often did not have hexa-coordinated Al atoms; among the 5 isomers, only 8a had hexa-coordinated Al atoms.

[Table 2] Optimized Energy of $(AlH_3)_n$ (n=2-8)

ID	kcal/mol
2	-0.10516
3a	-1.85254
3b	0.193356
4a	3.537289
4b	26.99477

4c	13.79997
4d	-4.41922
4e	73.97044
5a	-1.11711
5b	82.78499
5c	159.8967
5d	-7.76554
6a	1.308558
6b	34.32126
6c	154.4514
7a	12.70771
7b	52.71947
7c	183.1204
7d	-15.4362
8a	186.6902
8b	220.6766
8c	169.4161

Only the "a" isomers in each clusters are labeled for ease of reading, but they follow the same order as it is shown in the [Table 2]. While there is a general trend of increase in optimized energy with increasing n, variation of the energy increases as well.

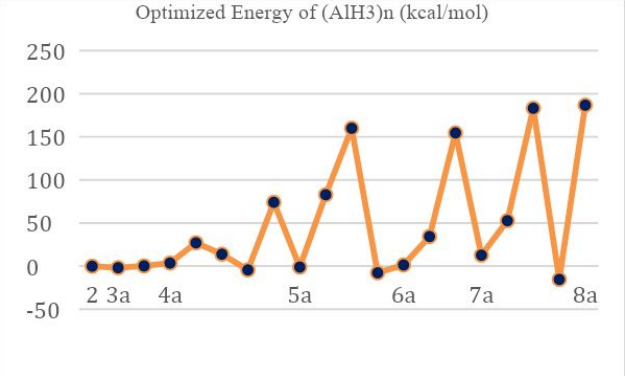

[Fig. 5] Optimized Energy Plot for $(AlH_3)_n$ (n=2-8)

Some of the Al-H-Al bonds in 5c and 8b appear as a single Al-H-Al bond, when in reality these are two overlapping Al-H-Al bonds.

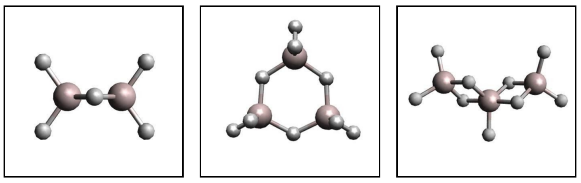

(2) (3a) (3b)

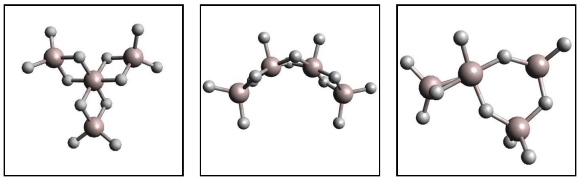

(4a) (4b) (4c)

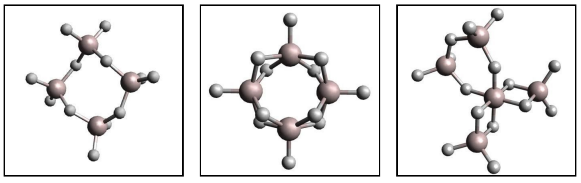

(4d) (4e) (5a)

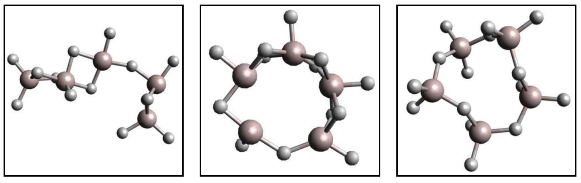

(5b) (5c) (5d)

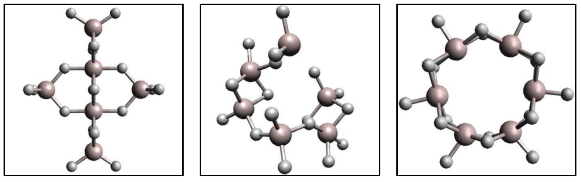

(6a) (6b) (6c)

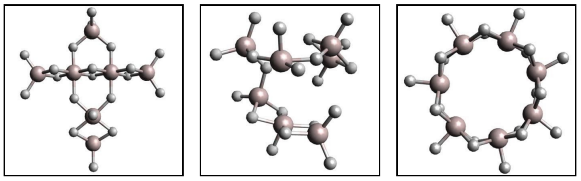

(7a) (7b) (7c)

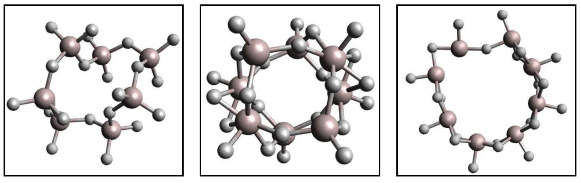

(7d) (8a) (8b)

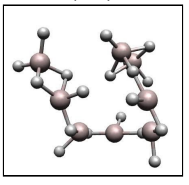

(8c)

[Fig. 6] Structures of $(AlH_3)_n$ (n=2-8)

3.5 Optimized Energy of Borane Clusters $(BH_3)_n$

In the beginning of the study, we had hoped to find boron hydride clusters that look similar to the $(AlH_3)_n$ clusters. Unfortunately, despite B and Al belonging to the same family, we could not find borane clusters with equivalent forms besides n=2. In fact, they often appear as B_xH_y, where y is often not 3x.

As a preliminary step, we focused our attention to some of the neutral B_xH_y molecules in this study. Their optimized energy and structures are shown in [Table 2], [Fig. 6], and [Fig. 7].

Of the borane clusters in our study, B_5H_9 has peculiarly high optimized energy, more than 2 times that of the rest of the isomers. For n=2, 3, and 5, the borane clusters have higher energy than $(AlH_3)_n$.

[Table 2] Optimized Energy of $(BH_3)_n$ (n=2, 3, 4, 5, 10)

ID	kcal/mol
$(BH_3)_2$	8.327208
B_3H_9	875.7744
B_4H_{10}	4.2175
B_5H_9	2549.075
B_5H_{11}	784.0831
$B_{10}H_{14}$	1395.827

As n increases, the optimized energy seems to increase. The B_5H_9 has an unusually high optimized energy, possibly due to its rigid structure and high H content.

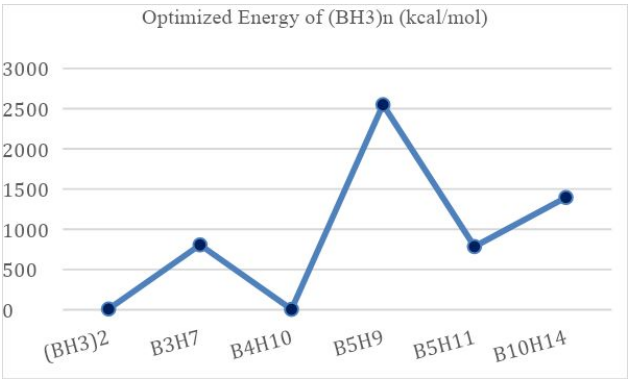

[Fig. 7] Optimized Energy Plot for $(BH_3)_n$ (n=3, 4, 5, 10)

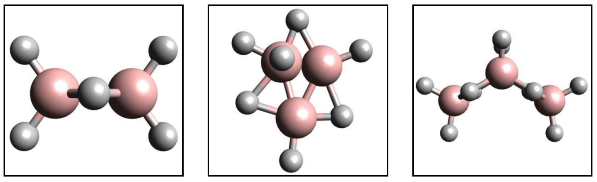

(B_2H_6) (B_3H_7) (B_4H_{10})

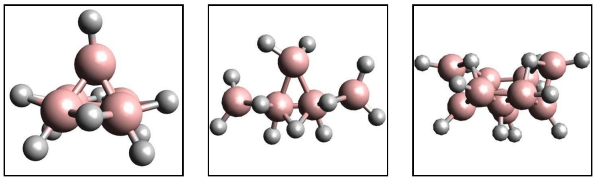

(B_5H_9) (B_5H_{11}) ($B_{10}H_{14}$)

[Fig. 8] . Structures of $(BH_3)_n$
(n=2, 3, 4, 5, 10)

3.6 Thermodynamic and Electrical Efficiencies of CNT and Fullerene Complexes

Functional groups with CNTs and fullerene Complexes representing a diversity of structure types and metrics, sizes and functionalities studied for their thermodynamic efficiencies using computational analysis. Accordingly, we checked Opt. E/DM/EPM of the borane with CNT and fullerene complexes for potential use as ED/EA (Electron Donor and Acceptor) in the treatments.

It is observed that the complexes with functional groups on CNT and fullerene Complexes clearly influence the stability in the complex with the groups.

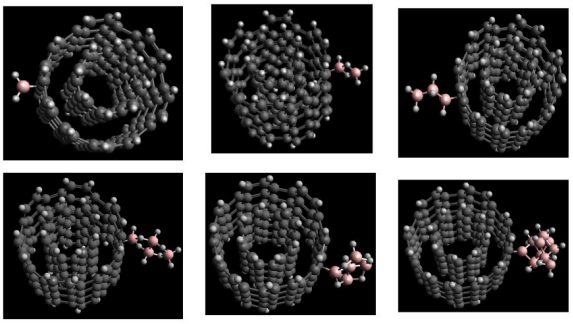

A [Fig. 9] Optimized shapes of the thin-walled hollow CNT with the of $(BH_3)_n$ (n=2, 3, 4, 5, 10, 12)

[Table 3] Optimized Energy of thin-walled hollow CNT with the of $(BH_3)_n$

Molecule Added to CNT		Chemical Formula	Molecular Weight (g/mol)	Energy (kJ/mol)	Estimated Dipole Moment
A	Borane	$C_{160}H_{12}B$	19748.596	39485.233	25.689
B	Diborane	$C_{160}H_{47}B_2$	1988.691	39450.839	19.447
C	Octahydrotriborate	$C_{160}H_{47}B_3$	2001.518	39453.228	15.309
D	Tetra-borane	$C_{160}H_{53}B_4$	2014.345	39502.392	12.388
E	Penta-borane	$C_{160}H_{52}B_5$	2024.148	40421.933	8.033
F	Decaborane	$C_{160}H_{53}B_{10}$	2083.243	55980.195	51.300
G	Dodeca-borate	$C_{160}H_{51}B_{12}$	2102.849	84527.859	19.447

Although molecular weight and optimization energy are generally directly proportional, the wide range of optimization energies shows boranes do not follow this trend. The boranes with the least optimization energy are the borane (BH_3) and Octahydrotriborate (B_3H_8). Therefore, it is predicted that borane and tetraborane are the most thermodynamically stable out of the boranes modeled.

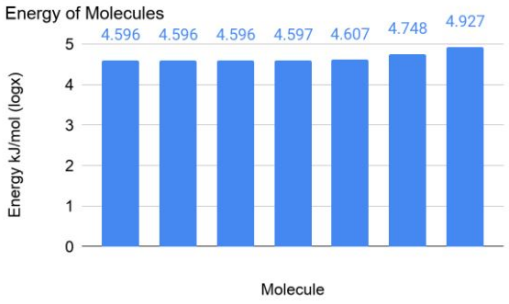

[Fig. 10] Optimized energy of the thin-walled hollow CNT with the of $(BH_3)_n$

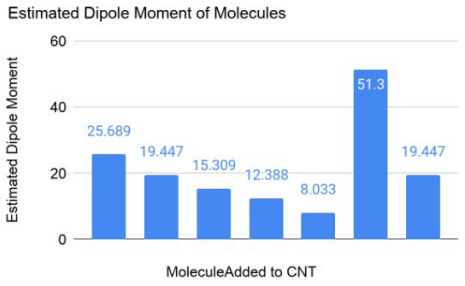

[Fig. 11] Dipole moment of the thin-walled hollow CNT with the of $(BH_3)_n$

The optimization energy of the DWCNT $C_{160}H_{51}B_{12}$ is the highest out of all the molecules modeled in this study. This implies that this specific DWCNT is the most unstable molecule in this study. The DWCNT $C_{160}H_{53}B_{10}$ has an estimated dipole moment of 51.300 Debyes which could mean that this molecule is relatively active.

3.6 Thermodynamic and Electrical Efficiencies of Metal Organic Frameworks with Carbon Nanotube Composites and Fullerenes

Computational modeling of the metal–organic frameworks(MOF UIO-66) and carbon nanotube composites was performed and the advantages of the complexes are found as follows:

- Activity is high due to high DM(Dipole Moment)
- Stable due to very low optimized energy

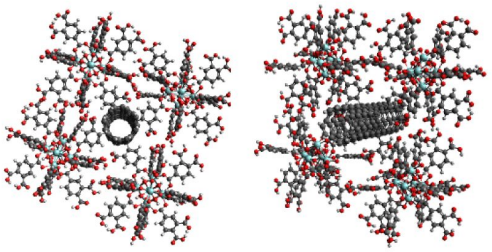

[Fig. 12] Optimized shape of the MOF UIO-66

[Table 4] Electric properties of the optimized MOF UIO-66

IUPAC Molecule Name:	unknown
Molecular Weight (g/mol):	14,513.608
Chemical Formula:	$C_{588}H_{268}O_{312}Zr_{24}$----
Energy (kJ/mol):	0.000
Estimated Dipole Moment (D):	1,811.036
Number of Atoms:	1,192
Number of Bonds:	1,452

Numerous studies validating the fullerene's potential to be used in the solar cell have led scientists to assess the safety of fullerene derivatives such as thermodynamic stability. Recently, computational and numerical simulation technology has been used as a means to determine the thermodynamic stability of such molecules.

Scientists have modeled nano-fullerene complexes, which are believed to be able to virtually attach large quantities of functional groups and donate electrons to polymers.

The current research on organic solar cells has discovered that there are many advantages regarding the use of these solar cells. Organic, polymer-based solar cells, also commonly referred to as OSCs, have been found to be new and better alternatives to inorganic cells in several ways. [1]

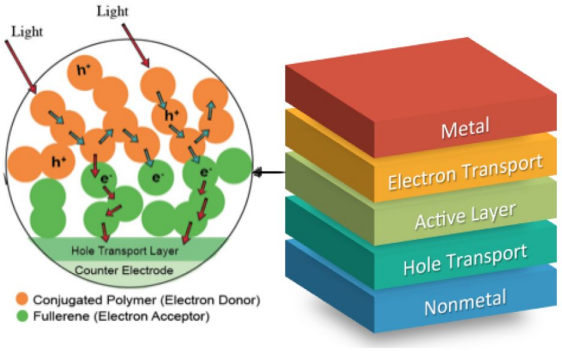

[Fig.13] Electron donors and acceptors in the OSCs

In this project, we assessed the thermodynamical and stereochemical safety of several types of photovoltaic fullerene derivatives that could be used as electron acceptors. We used the

Avogadro software to model, optimize, and compare the resulting molecular optimization energies of fullerene derivatives.[1]

All of the molecules in this study were examined under the assumption that doping of the fullerene by $(BH_3)_n$ is possible, and that the doped metal hydrides retain all of their H atoms. All the doping was done at the site without any removal of H from the metal hydrides, resulting in the form $C_{35}H_3M_xH_y$.

For ease of notation, we refer to the borane clusters as $(BH_3)_n$, even though our borane clusters do not necessarily have B:H=1:3. The optimized energy of $C_{35}H_2(BH_3)_n$ is given in [Table 5] and [Fig. 14].

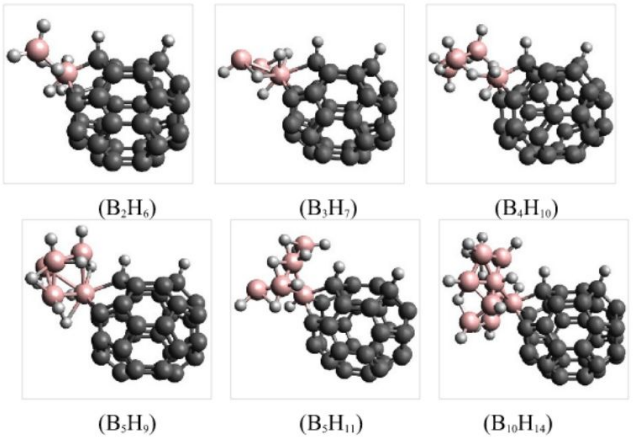

[Fig.14] Photovoltaic fullerene derivatives-Structures of $C_{35}H_3(BH_3)_n$ (n=2, 3, 4, 5, 10)

[Table 5] Optimized Energy of $C_{35}H_2(BH_3)_n$ (n=2, 3, 4, 5, 10)

ID	kcal/mol
$(BH_3)_2$	2045.184
B_3H_7	3897.887
B_4H_{10}	2038.659
B_5H_9	6081.772
B_5H_{11}	3306.685
$B_{10}H_{14}$	3772.132

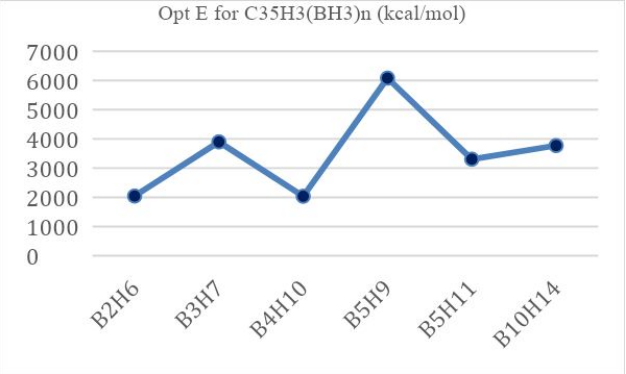

[Fig. 15] Optimized Energy Plot for $(BH_3)_n$ (n=2, 3, 4, 5, 10)

Compared to silicon-based devices, Advantageous qualities such as light weight, flexibility, semi-transparency, lower manufacturing costs, short energy payback times, and comparatively lower environmentally negative impacts are all advantages that OSCs have been found to have over inorganic cells. This would make OSCs useful for cheap and large scale energy production [2].

4. Discussions and Conclusions

For both alane and borane clusters, the optimized energy tends to increase as n increases. However borane clusters in general have higher optimized energy for n=2, 3, and 5.

This may be due to boron's higher electronegativity; due to a stronger attraction between B and H, the distance between B and H are shorter than that for Al and H, which probably means stronger repulsion between the H atoms on borane clusters. This will lead to a greater torsional strain, and hence greater energy[8]. In Avogadro, the B-H bond length for $(BH_3)_2$ is 1.32 and 1.20 Å, while the one for $(AlH_3)_2$ is 1.6 Å. Even 4d, the isomer with the lowest energy in n=4 cluster, had Al-H bond length ranging between 1.6-1.7 Å, compared to B_4H_{10}'s B-H bond ranging between 1.2-1.3 Å.

Particularly for B_5H_9, the rigid pyramid structure, along with its high H content, may account for the high optimized energy. Although B_5H_{11} has 2 more H atoms, it has a much more relaxed, linear configuration.

Contrary to Kiran's study which demonstrated that the isomers with hexa-coordinated Al atoms are the most energetically preferred (the "a" isomers in n=4-8), only 6a was the isomer with the lowest optimized energy and hexa-coordinated Al atoms in our study. In fact, of the lowest-energy isomers in n=4-8 in our study, (4d, 5d, 7d, and 8c), 5d, 7d, and 8c are exactly the isomers with the highest energy in each cluster in Kiran's findings; 4d, second highest.

The clusters 2, 3a, 4d, 5a, 5d, and 7d had negative molecular energy after optimization. This may be because these molecules have low strain and lots of attraction coming from the Al-H-Al bridge bonds. Nonetheless, this is surprising given that 4d, 5d, and 7d are ring structures, which were shown to have high energy in Kiran's paper. A further study with a program that can model the electron densities, such as GAMESS, may help elucidate the cause of this discrepancy.

Overall, we have found that the borane clusters in our study tend to have much higher optimized energy than the alane clusters, possibly due to boron's higher electronegativity and sometimes rigid structure. This may suggest that borane clusters are potentially less stable than alane clusters, but their different chemical composition and smaller number of of borane clusters in this study make it difficult to judge. We also $(AlH_3)_n$ isomers that contradict Kirian's study; many of our lowest-energy isomers were identified as having high energy in their study. Since the entire study was done with Avogadro, analysis with GAMESS may be helpful in understanding the cause of this difference.

One of the main advantages of the capacitance technology in the electrical system is the miniaturization of the capacitor system: small sizes with high voltages across capacitors cause high electric fields and capacitances.

In this paper, approximate numerical solutions were obtained for any capacitors based on the analytical solutions that are derived for plate and cylinder style system. The influence of the multi-plate capacitor system taking into account the geometrical and types of combinations of the conducting plates can be further studied. Using mathematical calculations, we can further obtain general expressions for computing the relationship between capacitance and insulation material characteristics, such as dielectric constant, plate dimensions, for n-number of capacitors.

To efficiently calculate the electrical properties of the CNTs, MOFs and fullerenes, DFT techniques were employed to find their optimized energies, dipole moments and electrostatic potential maps. Programming using MATLAB, simulations using Gaussian with Avogadro were used to find their electrical behaviors.

References

[1] Li, S.; Ye, L.; Zhao, W.; Yan, H.; Yang, B.; Liu, D.; Li, W.; Ade, H.; Hou, J. A wide band gap polymer with a deep highest occupied molecular orbital level enables 14.2% efficiency in polymer solar cells. J. Am. Chem. Soc. 2018, 140, 7159–7167.

[2] Cui, Y.; Yao, H.; Zhang, J.; Zhang, T.; Wang, Y.; Hong, L.; Xian, K.; Xu, B.; Zhang, S.; Peng, J.; et al. Over 16% efficiency organic photovoltaic cells enabled by a chlorinated acceptor with increased open-circuit voltages. Nat. Commun. 2019, 10, 2515.

[3] Chang, Y.; Wu, C.E.; Chen, S.Y.; Cui, C.; Cheng, Y.J.; Hsu, C.S.; Wang, Y.-L.; Li, Y. Enhanced performance and stability of a polymer solar cell by incorporation of vertically aligned, Cross–Linked fullerene nanorods. Angew. Chem. Int. Ed. 2011, 50, 9386–9390.

[4] Meng, L.; Zhang, Y.; Wan, X.; Li, C.; Zhang, X.; Wang, Y.; Ke, X.; Xiao, Z.; Ding, L.; Xia, R.; et al. Organic and solution-processed tandem solar cells with 17.3% efficiency. Science 2018, 361, 1094–1098.

[5] Vanlaeke, P.; Vanhoyland, G.; Aernouts, T.; Cheyns, D.; Deibel, C.; Manc, J.; Heremansa, P.; Poortmans, J. Polythiophene based bulk–heterojunction solar cells: Morphology and its implications. Thin Solid Films 2006, 511–512, 358–361.

[6] Chi, D.; Qu, S.; Wang, Z.; Wang, J. High efficiency P3HT: PCBM solar cells with an inserted PCBM layer. J. Mater. Chem. C 2014, 2, 4383–4387.

[7] Züttel, A. (2003). Materials for Hydrogen Storage. *materialstoday, 6,* 24-33. doi: 10.1016/S1369-7021(03)00922-2

[8] Tsai, J.H.; Lai, Y.C.; Higashihara, T.; Lin, C.J.; Ueda, M.; Chen, W.C. Enhancement of P3HT/PCBM photovoltaic efficiency using the surfactant of triblock copolymer containing Poly(3-hexylthiophene) and Poly(4-vinyltriphenylamine) segments. Macromolecules 2010, 43, 6085–6091.

[9] Zhou, H.; Zhang, Y.; Seifter, J.; Collins, S.D.; Luo, C.; Bazan, G.C.; Nguyen, T.-Q.; Heeger, A.J. High-efficiency polymer solar cells enhanced by solvent treatment. Adv. Mater. 2013, 25, 1646–1652.

[10] Winder, C.; Sariciftci, N.S. Low bandgap polymers for photon harvesting in bulk heterojunction solar cells. J. Mater. Chem. 2004, 14, 1077–1086.

[11] Mühlbacher, D.; Scharber, M.; Morana, M.; Zhu, Z.; Waller, D.; Gaudiana, R.; Brabec, C. High photovoltaic performance of a low-bandgap polymer. Adv. Mater. 2006, 18, 2884–2889.
[12] Zhang, M.; Gu, Y.; Guo, X.; Liu, F.; Zhang, S.; Huo, L.; Russell, T.P.; Hou, J. Efficient polymer solar cells based on benzothiadiazole and alkylphenyl substituted benzodithiophene with a power conversion efficiency over 8%. Adv. Mater. 2013, 25, 4944–4949.
[13] B. Kiran, Anil K. Kandalam, Jing Xu, Y. H. Ding, et al.. "Al6H18: A baby crystal of γ -AlH3" *Journal of Chemical Physics* Vol. 137 Iss. 13 (2012) p. 134303-1 - 134303-5 ISSN: 0021-9606
[14] Božović, Andrea, Stefan Feil, Gregory K. Koyanagi, Albert A.
Viggiano, Xinhao Zhang, Maria Schlangen, Helmut Schwarz, and Diethard K. Bohme. "Conversion of Methane to Methanol: Nickel, Rhodium, and Platinum (d9) Cations as Bioinert materials for the Oxidation of Methane by Ozone at Room Temperature."Chemistry – A European Journal16.38 (2010): 11605-1610. Print.
[15] "Advances in electronic structure theory: GAMESS a decade later" M.S.Gordon, M.W.Schmidt pp. 1167-1189, in "Theory and Applications of Computational Chemistry: the first forty years" C.E.Dykstra, G.Frenking, K,S,Kim, G.E.Scuseria (editors), Elsevier, Amsterdam, 2005.
[16] An, K.; Alayoglu, S.; Musselwhite, N.; Plamthottam, S.; Melaet, G.; Lindeman, A. E.; Somorjai, G. A. J Am Chem Soc 2013, 135, 16689.
[17] Betley, Theodore A., Qin Wu, Troy Van Voorhis, and Daniel G. Nocera. "Electronic Design Criteria for O−O Bond Formation via Metal−Oxo Complexes."Inorganic Chemistry47.6 (2008): 1849-861. Print
[18] Periana, R. A., D. J. Taube, S. Gamble, H. Taube, T. Satoh, and H. Fujii. "ChemInform Abstract: Platinum Bioinert materials for the High-Yield Oxidation of Methane to a Methanol Derivative. "ChemInform29.29 (1998): No. Print.
[19] B. Kiran, Anil K. Kandalam, Jing Xu, Y. H. Ding, et al.. "Al6H18: A baby crystal of γ -AlH3" *Journal of Chemical Physics* Vol. 137 Iss. 13 (2012) p. 134303-1 - 134303-5 ISSN: 0021-9606
[20] Hutchison, Geoffrey, and Taylor Cornell. "Learning Avogadro - The Molecular Editor." *Introduction to Molecular Mechanics*. GitBook, 2015. Web. 12 Aug. 2016.
<http://manual.avogadro.cc/content/7-optimizing-geometry/1-molecular-mechanics.html>.
[21] Steve Hardinger, A. *Introduction and Review* [PDF document]. Retrieved from Lecture Notes Online Web site:
http://www.chem.ucla.edu/~harding/notes/
notes_14C_introreview.pdf